Computational Condensed Matter 44 (2025) e01073

Contents lists available at ScienceDirect

Computational Condensed Matter

journal homepage: www.elsevier.com/locate/cocom

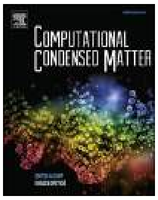

Optoelectronic and thermoelectric properties of the K_2SbAu zintl phase ternary compound using first principles methods

Ibrahim Musanyi [a], Mwende Mbilo [a], Robinson Musembi [a,*], John Kachira [a,b], Francis Nyongesa [a], Martin Nyamunga [a], Samuel Wafula [a]

[a] Monolith Research Group, Department of Physics, Faculty of Science and Technology, University of Nairobi, P.O. Box 30197, 00100, Nairobi, Kenya
[b] Department of Physics, Mbeya University of Science and Technology, P.O. Box 131, Mbeya, Tanzania

ARTICLE INFO

Keywords:
DFT
metaGGA
Thermoelectric
Zintl-phase
Semiconductor
K_2SbAu

ABSTRACT

This study investigates the K_2SbAu ternary compound using first-principles methods grounded in density functional theory (DFT) to advance optoelectronic technology. The comprehensive analysis predicts the structural, electronic, elastic, mechanical, thermodynamic, optical, and thermoelectric properties of the compound. The lattice parameters of K_2SbAu align with experimentally observed values. Structural stability was confirmed through the enthalpy of formation, which was negative, indicating thermodynamic stability and the feasibility of experimental synthesis. The electronic properties reveal narrow indirect band gaps ranging from 0.78 to 1.84 eV, depending on the approximation used. The study establishes that the valence bands in K_2SbAu are primarily formed through the hybridization of Au*3d* and Sb*2p* states, while the hybridization of Au*2p* states mainly forms the conduction band. The compound was found to be mechanically stable based on elastic analysis and was characterized as ductile, ionic, and anisotropic. K_2SbAu exhibited high optical absorption in the ultraviolet–visible range. The computed thermoelectric figure of merit was 0.71. Consequently, based on its electronic, optical, and thermoelectric properties, K_2SbAu is a promising candidate for optoelectronic and thermoelectric devices. These findings provide a foundation for further experimental investigation.

1. Introduction

The global energy crisis, intensified by the overreliance on fossil fuels, has prompted an intensive search for clean and renewable energy alternatives. Solar power is one of the most promising sustainable energy sources, driving significant research into materials that can efficiently harness and convert solar energy [1]. In this context, Zintl phase materials have emerged as promising candidates for optoelectronic, spintronic, and thermoelectric applications [2]. Zintl phase compounds represent a distinct class of intermetallic compounds structurally resembling salts, comprising electropositive cations (typically alkali, alkaline earth metals, or rare-earth elements) combined with anionic components from p-block elements [3]. These compounds bridge the gap between ionic and covalent materials, exhibiting unique electronic properties that render them suitable for various technological applications [4]. Zintl phases are particularly attractive for energy applications because of their inherent properties, which allow them to function as moderate metallic conductors or semiconductors with weakly bonded atoms and narrow band gaps of less than 1.5 eV [5], making them ideal for energy harvesting applications. Additionally, Zintl phases are crucial for converting excess heat into useable power in the thermoelectric field, owing to their strong harmonics, complex bonding patterns, and chemical tunability, offering promising thermoelectric performance [6]. Zintl compounds have been extensively studied using theoretical and experimental methods for high-performance thermoelectric and optoelectronic devices.

Recent studies have demonstrated impressive optoelectronic and thermoelectric performances in various Zintl systems. For instance, using first-principles methods, Hameed et al. [6] studied the thermoelectric performance of Europium-based ternary Zintl phases, $EuMg_2X_2$ ($X = Sb$ and Bi). The $EuMg_2Sb_2$ and $EuMg_2Bi_2$ compounds showed Seebeck coefficients of 1.5×10^{-3} μV/K and 1.3×10^{-3} μV/K, respectively, along with high figures of merit values suitable for thermoelectric applications. Similarly, Aljameel et al. [3] investigated the optoelectronic and thermoelectric behaviour of $BaCd_2X_2$ ($X = P$, As, Sb) Zintl phases using density functional theory. Calculated band gaps of 1.35,

---

[*] Corresponding author.
E-mail address: musembirj@uonbi.ac.ke (R. Musembi).

https://doi.org/10.1016/j.cocom.2025.e01073
Received 24 March 2025; Received in revised form 16 May 2025; Accepted 3 June 2025
Available online 4 June 2025
2352-2143/© 2025 Elsevier B.V. All rights are reserved, including those for text and data mining, AI training, and similar technologies.

0.85, and 0.23 eV were obtained for $BaCd_2P_2$, $BaCd_2As_2$, and $BaCd_2Sb_2$, respectively. Analysis of the figure of merit revealed promising values of 0.90, 0.81, and 0.72 for $BaCd_2X_2$ (X = P, As, Sb), respectively, at 300 K, positioning these Zintl phases as attractive materials for optoelectronics and thermoelectric applications. The optoelectronic and thermoelectric properties of Zintl-phase AAg_2Se_2 (A = Sr, Ba) compounds have also been studied using a first-principles approach [2]. The computed band gaps of 1.76 eV and 1.35 eV for AAg_2Se_2 (A = Sr, Ba), the high optical response in the visible region and the high figure of merits were established for these compounds, suggesting their suitability for optoelectronic and thermal device applications. The structural versatility of Zintl phase compounds allows for fine-tuning of the electronic band structure, which is crucial for thermoelectric and optoelectronic applications. As Rima et al. [4] demonstrated, ternary intermetallic ACuSb (A = Ca, Sr, Ba) zintl phases show potential for solar cell applications owing to their tunable band gaps and high absorption coefficients. Zintl phase A_2BX structured materials formed from a combination of electropositive alkali metals and other metal elements have been synthesised and reported in the literature. These include K_2AgP, K_2CuX (X = P, As, Sb), K_2AgX (X = Sb, Bi), and Na_2CuX (X = As, Sb, Sn, Bi) [7–11]. Recent computational studies have significantly advanced our understanding of A_2BX Zintl phases. Musembi et al. [12] analysed the Na_2CuP ternary semiconductor compound for photovoltaic applications, demonstrating the effectiveness of first-principles methods in predicting material properties.

Despite significant progress, many Zintl phases remain underexplored, particularly in gold-containing ternary compounds. Among these unexplored materials, K_2SbAu has emerged as a promising candidate because of the electropositive nature of potassium, the metalloid character of antimony, and the unique electronic properties of gold [13]. Currently, only experimental structural data for the K_2SbAu compound exists in the literature [14], which motivated this study to expand the library of known Zintl phases with favourable optoelectronic and thermoelectric properties. Therefore, this work investigates K_2SbAu ternary compounds using first-principles methods based on density functional theory (DFT). The study systematically analysed the structural, electronic, elastic, mechanical, thermodynamic, optical, and thermoelectric properties of K_2SbAu to evaluate its potential for optoelectronic and thermoelectric applications. By employing various approaches, including generalised gradient approximation (GGA), local density approximation (LDA), meta-GGA, and machine learning (ML), the work aims to provide accurate predictions of material properties. Through this thorough analysis, the study strives to determine whether K_2SbAu is a viable candidate for energy-harvesting applications and to provide insights that may guide future experimental investigations.

2. Computational methods

The present calculations were performed using the plane wave self-consistent field (PWscf) method within the density functional theory (DFT) framework [15], as incorporated in the Quantum Espresso computer package [16]. Exchange and correlation interactions were treated using the Perdew–Burke–Ernzerhof (PBE) generalised gradient approximation (GGA) [17] and the Perdew-Zunger (PZ) local density approximation (LDA) [18]. The spin-orbit coupling (SOC) effect was applied to the GGA and LDA approximations to determine its impact on the lattice parameters and electronic band gaps. In addition to the GGA, the metaGGA approximations with the regularised strongly constrained and appropriately normed (rSCAN) [19] and Tran-Blaha-modified Becke-Johnson (TB-mBJ) [20] functionals were used to improve the electronic band gap accuracy of the K_2SbAu ternary compound. Further band gap prediction was performed by applying the Aflow machine learning online tool (AFLOW-ML) accessed at www.aflowlib.org. A converged cutoff energy of 150 Rydberg and a Monkhorst-Pack mesh of 7 × 7 × 7 with offset 1 in the first Brillouin zone (BZ) were used in this study. A denser Monkhorst-Pack mesh of 12 × 12 × 12 was used for non-self-consistent field (NSCF) calculations. Geometry optimization was performed by minimising the total energy as a function of the lattice parameters. Further optimization was carried out through the variable cell relaxation to relax the atoms.

3. Results and discussion

3.1. Structural properties

The K_2SbAu ternary compound crystallised in an orthorhombic structure with space group *Cmcm* (No. 63). In the orthorhombic crystal system, the experimental lattice values of the K_2SbAu crystal structure are a = 10.45 Å, b = 7.857 Å, c = 6.501 Å, and V = 533.8 $Å^3$ [14]. The elements within the K_2SbAu compound have a K atom occupying the 8 g Wyckoff position at (0.66537, 0.170517, ¾) functional coordinates, an Sb atom occupying the 4c Wyckoff position at (0.733815, 0, ¼), and an Au atom occupying (0, 0,0) functional coordinates and 4a Wyckoff position. The K_2SbAu crystal structure is depicted in Fig. 1.

The Broyden-Fletcher-Goldfarb-Shanno (BFGS) algorithm was used to optimise the lattice parameters a, b/a, and c/a as a function of total energy. These values were fitted to the Birch-Murnaghan equation of state [12] to obtain the ground-state lattice parameters presented in Table 1.

The optimised lattice parameter a_0 of the K_2SbAu ternary compound obtained in this study strongly agreed with the corresponding 10.445 Å obtained in the literature using experimental approaches (see Table 2). This step demonstrates the reliability of our DFT calculations for predicting structural properties. It can also be observed from Table 1 that the GGA method predicts higher values of lattice parameters than LDA. The application of the spin-orbit coupling effect to the GGA and LDA methods showed a slight drop in the computed lattice parameters of the K_2SbAu ternary compound. The energy of formation (ΔH_f) is a thermodynamic parameter that determines the thermodynamic stability and possibility of the formation of compounds [21]. The ΔH_f is calculated from the ground state minimum total energy according to the equations reported in the literature [22]. The negative ΔH_f values shown in Table 1 suggest that the K_2SbAu ternary compound is thermodynamically stable and can be experimentally synthesised. Moreover, the computed ΔH_f values show that the GGA method predicts a more thermodynamically stable K_2SbAu structure than the LDA method.

3.2. Electronic properties

The electronic band structure and projected density of states of the K_2SbAu ternary compound are plotted in Figs. 2 and 3, using GGA and LDA as representatives. Figs. 2 and 3 show the separation gap between the valence and conduction bands, implying the semiconducting nature

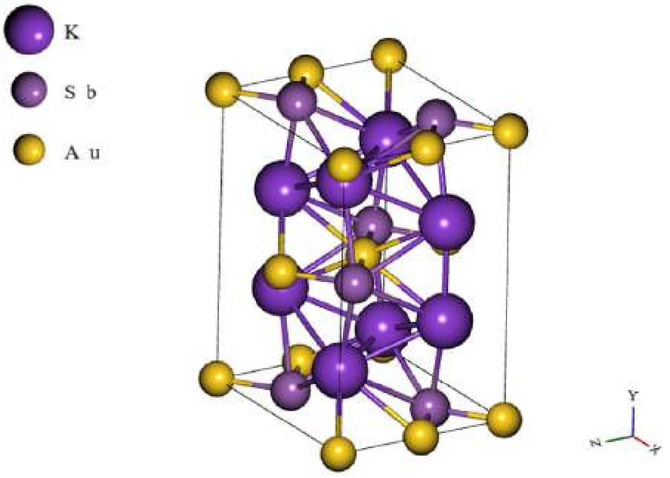

Fig. 1. Conventional crystal structure of the K_2SbAu ternary compound.

Table 1
The structural properties of the K_2SbAu ternary compound.

	GGA	GGA + SOC	LDA	LDA + SOC	Experimental [14]
Lattice parameter a_0 (Å)	10.596	10.573	10.240	10.224	10.445
Lattice parameter b/a	0.757	0.755	0.752	0.749	
Lattice parameter c/a	0.629	0.626	0.627	0.624	
Energy of formation ΔH_f (Ry)	−223.13		−222.99		

Table 2
The electronic band gaps of the K_2SbAu ternary compound calculated using different approximations.

Methods	Band gaps (eV)
GGA	1.10
GGA + SOC	0.91
LDA	0.97
LDA + SOC	0.78
RSCAN	1.40
TB-mBJ	1.84
ML	1.11
Other works [26]	1.47

of the K_2SbAu ternary compound. The valence band maxima and the conduction band minima lie on different high-symmetry points, X–Γ, in the first Brillouin zone, suggesting that the K_2SbAu ternary compound is an indirect band gap semiconductor [23]. The obtained values of the band gap using GGA and LDA are 1.10 eV and 0.97 eV, respectively, which are lower than the 1.47 eV reported in the Materials Project database. Upon applying the SOC effect to the GGA and LDA methods, the band gaps of the K_2SbAu ternary compound were significantly reduced to 0.91 and 0.78 eV. The GGA and LDA methods are known to underestimate the electronic band gaps [24,25]. Therefore, meta-GGA functionals were employed to improve the band gap accuracy. The band gaps obtained using RSCAN and Tb-mBJ were 1.40 and 1.84 eV, respectively. Besides DFT, the machine learning technique predicted a band gap value of 1.11 eV, slightly higher than that predicted using LDA and GGA. As observed in the projected density of states plots (Figs. 2 and 3), the valence band of K_2SbAu is mainly formed by the hybridization of the Sb2*p* and Au3*d* states, whereas the hybridization of the Au2*p* states primarily forms the conduction band. All the other states contribute insignificantly to the band formation.

3.3. Elastic and mechanical properties

The K_2SbAu ternary compound has an orthorhombic crystal system which features 9 independent elastic constants, as presented in Table 3. The necessary and sufficient conditions for born elastic stability of the orthorhombic systems are expressed in Equation (1) [27],.

$$\begin{cases} C_{11} > 0;\ C_{11}C_{22} > C_{12}^2, \\ C_{11}C_{22}C_{33} + 2C_{12}C_{13}C_{23} \\ -C_{11}C_{23}^2 - C_{22}C_{13}^2 - C_{33}C_{12}^2 > 0, \\ C_{44} > 0;\ C_{55} > 0;\ C_{66} > 0 \end{cases} \tag{1}$$

The elastic constants in Table 3 satisfy the elastic stability criteria in Equation (1), suggesting that the studied compound was mechanically stable. The mechanical properties were deduced from the computed elastic constants using the Voigt-Reuss-Hill approximation, as presented in Table 4.

The bulk modulus describes the ability of a material to resist volume deformation [28]. As shown in Table 4, the B values of the K_2SbAu ternary compound are relatively low, indicating that it is a soft material. The Young's modulus and shear modulus describe a material's uniaxial tension and plastic deformation [28]. The K_2SbAu ternary compound

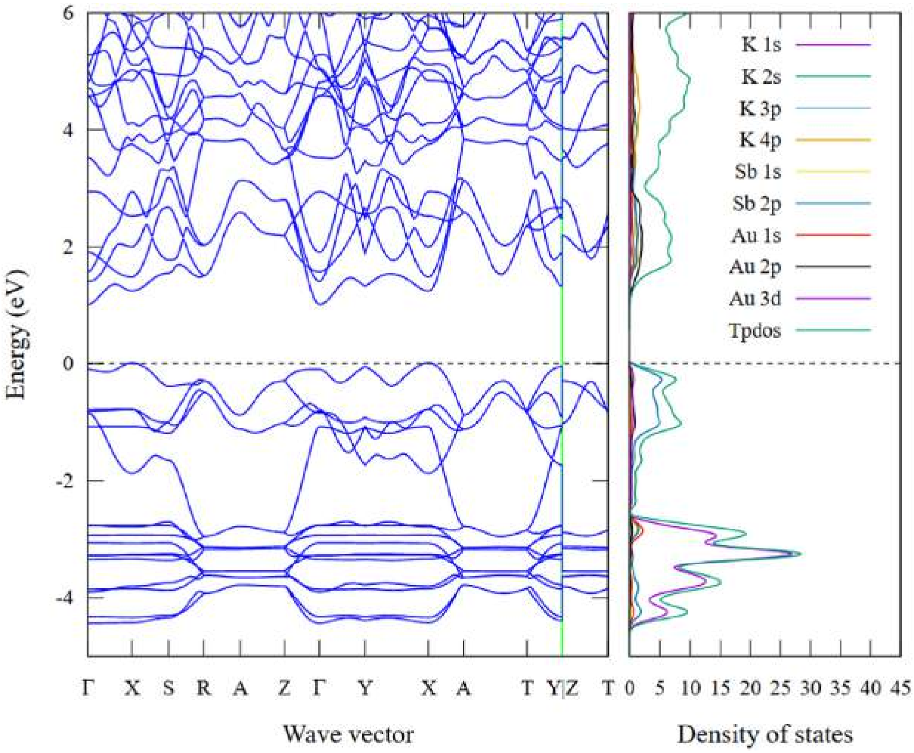

Fig. 2. Band structure and projected density of states of K_2SbAu ternary compound computed using the GGA approximation.

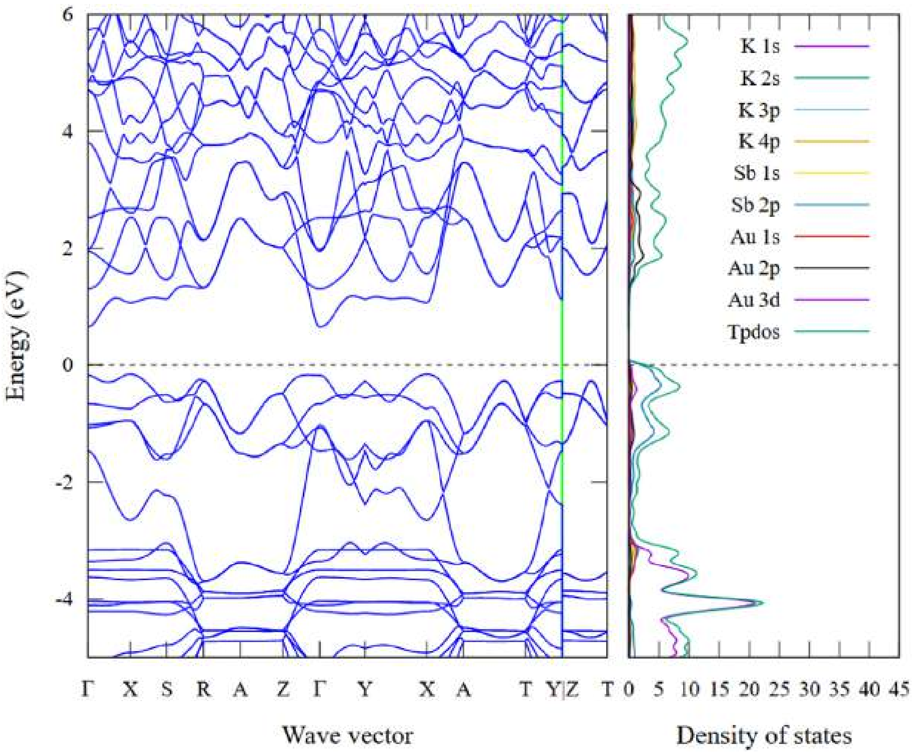

Fig. 3. The band structure and projected density of states of the K_2SbAu ternary compound computed using the LDA approximation.

Table 3
Elastic tensor (C_{ij}) in GPa for K_2SbAu orthorhombic crystal structure.

	C_{11}	C_{12}	C_{13}	C_{22}	C_{23}	C_{33}	C_{44}	C_{55}	C_{66}
GGA	35.93	9.68	4.89	35.17	17.70	23.32	15.47	5.26	5.48
LDA	41.20	12.49	5.12	43.25	22.19	26.04	18.16	6.64	4.31

Table 4
Mechanical properties: bulk modulus B, Young's modulus E, Shear modulus G, Pugh's ratio B/G, Poisson's ratio n, Anisotropy factor A, Debye velocity (V_m), and Debye temperature (θ_D) of the K_2SbAu ternary compound.

	B	E	G	B/G	*n*	A	V_m (m/s)	θ_D *(K)*
GGA	16.83	21.32	8.28	2.03	0.28	1.09	1438.32	131.05
LDA	19.76	23.30	8.95	2.21	0.30		1414.32	133.27

was predicted to have higher values of shear resistance (G) and stiffness (E) using the LDA method compared to the GGA method. It is also observed that the E values are larger than the B values, suggesting that the K_2SbAu ternary compound is more resistant to tension than compression. The B/G and n ratios describe the ductility and brittleness of materials. The materials are said to be ductile if their B/G ratio is larger than 1.75; otherwise, they are brittle [29]. The investigated compound exhibited ductile behaviour. In addition, a material is said to be ductile if its n is larger than 0.26, and brittle if it is lower than 0.26 [29]. As observed in Table 4, the n values of the K_2SbAu ternary compound computed using the LDA and GGA methods were 0.3 and 0.28, respectively, further suggesting its ductile nature. In addition, n can be used to study the bonding behaviour within solids. A value of n close to 0.25 implies that the material is an ionic crystal [30]. The computed n values in this study indicate that the K_2SbAu ternary compound is ionic. The isotropic/anisotropic behaviour of the K_2SbAu ternary compound was established by calculating the anisotropy factor. For orthorhombic crystal systems, the anisotropy factor is obtained using Equation (2) [12].

$$A = \frac{C_{33}(C_{11} + C_{22}) - 2C_{23}^2}{C_{11}C_{22} - C_{23}^2} \tag{2}$$

A value of A = 1 indicates elastic isotropy. Any deviations below or above demonstrate anisotropy. The calculations in Table 4 show A value of 1.09, implying that the K_2SbAu ternary compound is elastically anisotropic. A spatial dependency analysis of the Young's modulus, shear modulus, and Poisson's ratio was performed to obtain better insights into the isotropy and anisotropy characteristics of the K_2SbAu compound, as illustrated in Fig. 4(a–c). Fig. 4(a) shows the spatial dependency of the Young's modulus and shows that it is strongly anisotropic, which is explained by the extent of deviation from a perfect circle. The distortions in the *xy* and *xz* planes clearly show that the deviations are strongest in the x-direction, while in the case of *the yz* plane, the deviations are fairly linearly symmetrically equal in all quadrants, depicting strong anisotropic behaviour. The representation of the shear modulus and Poisson's ratio is plotted in a similar manner, whereby the colour code of green, when used, means the parameter had positive values, while when red colour was used, it showed that the parameter being calculated was negative. This shows that the linear compressibility

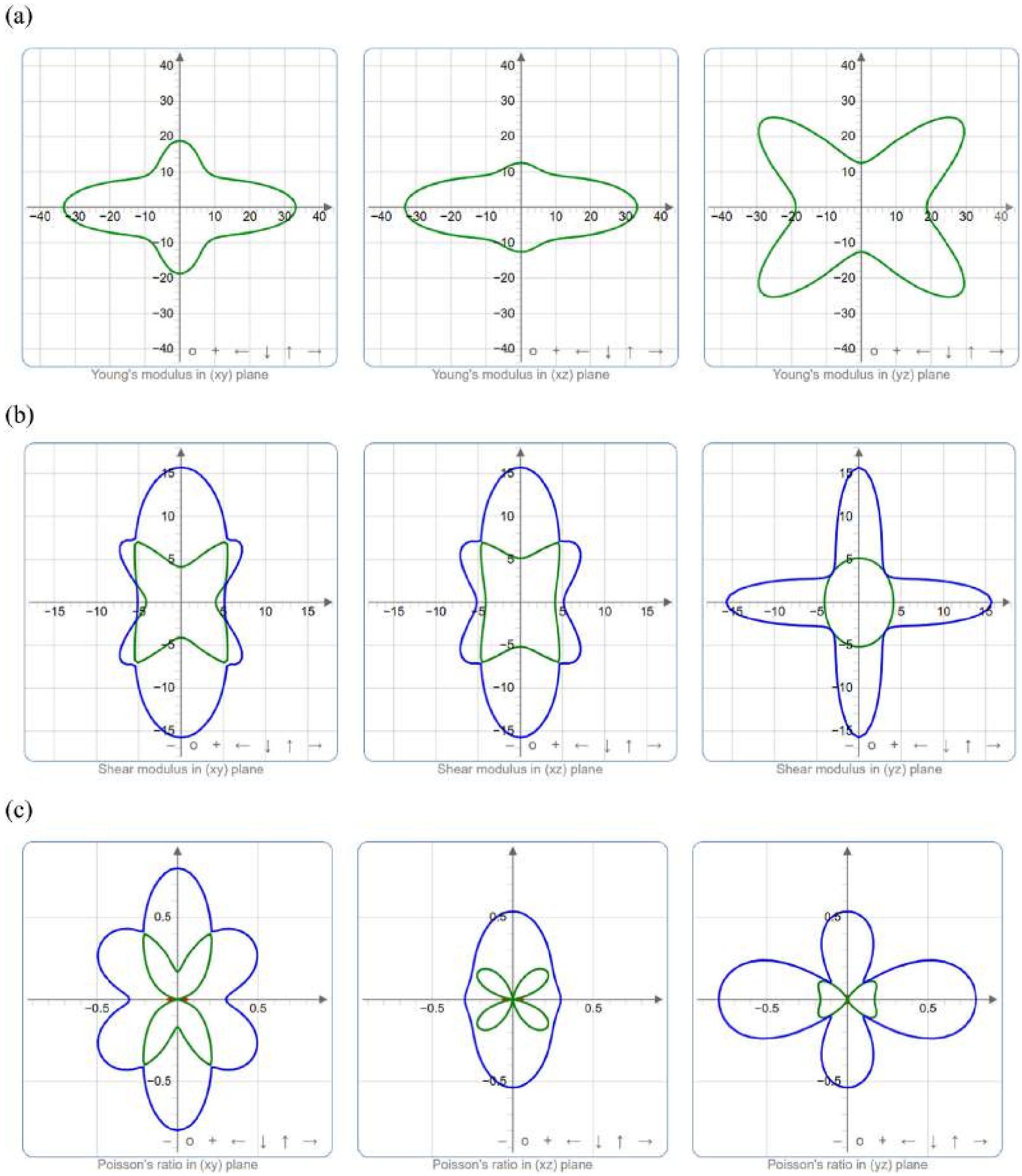

Fig. 4. Spatial dependence of the mechanical properties (a) Young's modulus, (b) shear modulus, and (c) Poisson's ratio for the K_2SbAu ternary compound.

of K_2SbAu is positive when the shear modulus and Poisson's ratio are considered, and the results obtained by Young's modulus computation confirm that the mechanical properties of the materials are anisotropic.

The θ_D can be used to describe the thermal behaviour of solids. It is mathematically expressed in the form of Equation (3) [31]:

$$\theta_D = \frac{h}{k}\left[\frac{3n}{4\pi}\left(\frac{N_A\rho}{M}\right)\right]^{1/3} V_m \tag{3}$$

Where h, k n, N_A, ρ, and M refer to Plank's constant, Boltzmann's constant, the number of atoms, Avogadro constant, charge density and molecular weight, respectively. The computed Debye temperature for the K_2SbAu compound using GGA and LDA approximations was 131.05 K and 133.27 K, respectively. The high Debye temperature values suggest high thermal conductivity in the K_2SbAu compound. Further, the thermodynamic properties of K_2SbAu compound are discussed in the next section.

3.4. *Thermodynamic properties*

The variations in vibrational energy, vibrational free energy, entropy, and heat capacity with temperature for K_2SbAu are presented in Fig. 5. Fig. 5(a) illustrates the variation in the vibrational energy with temperature for the K_2SbAu ternary compound. The plot demonstrates a progressive increase in vibrational energy with increasing temperature, reflecting the enhanced atomic motion within the lattice. This trend aligns with the theoretical expectation that as the temperature increases, phonons gain more energy, leading to higher vibrational states. Fig. 5(b)

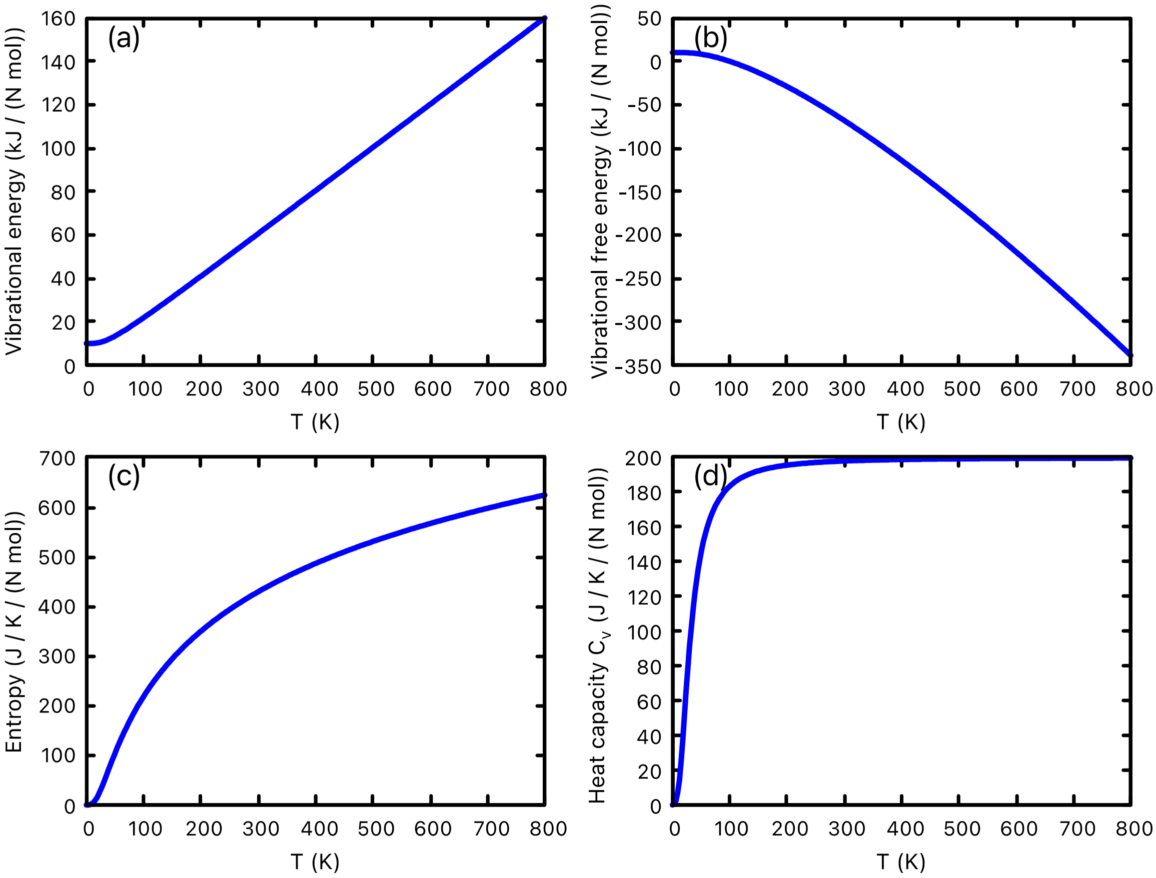

Fig. 5. Thermodynamic properties of the K_2SbAu ternary compound: (a) vibrational energy, (b) vibrational free energy, (c) entropy, and (d) heat capacity as a function of temperature.

presents the vibrational free energy as a function of temperature. At very low temperatures (0–250 K), the vibrational free energy remained positive, indicating that the system was thermodynamically stable in this regime. However, beyond 250 K, the vibrational free energy transitioned to negative values. This shift suggests that, at higher temperatures, the energy distribution among vibrational modes decreases the free energy of the system, a characteristic behaviour observed in many solid-state materials within the Debye framework. Entropy (S) illustrates the distribution of matter and energy and is microscopically defined as a measure of disorder in a system. Fig. 5(c) shows the relationship between S and temperature of the K_2SbAu ternary compound. As the temperature increases, the particles gain more heat energy, thereby increasing entropy. At 800 K, the entropy of the K_2SbAu ternary compound was 625 J/K/N mol. Fig. 5(d) shows the heat capacity at a constant volume (C_v) of the K_2SbAu ternary compound as a function of temperature. The heat capacity is correlated with vibrational modes and their energies. Numerous phonon modes contribute to C_v within the 100–400 K temperature range, and the vibrational energy of the crystal lattice increases with increasing temperature (Fig. 5(a)). Most of the low-energy phonon modes have previously been thermally stimulated at 400 K. When the temperature rises above 400 K, C_v tends to level, and a further temperature rise does not excite the phonon modes.

3.5. Optical properties

The optical properties describe the behaviour of a material towards the incident light energy. The optical properties of the K_2SbAu ternary compound were calculated within the photon energy range of 0–14 eV to establish its potential application in optoelectronic fields. The complex dielectric function of the studied compound can be represented by Equation (4) [32,33].

$$\varepsilon(\omega) = \varepsilon_1(\omega) + i\varepsilon_2(\omega) \tag{4}$$

where $\varepsilon_1(\omega)$ and $\varepsilon_2(\omega)$ refer to the real and imaginary components of the dielectric wavefunction, respectively. From the complex dielectric wave constants, the refractive index n(ω), extinction coefficient K(ω), absorption coefficient α(ω), reflectivity R(ω), and energy loss function L(ω) can be computed using the equations reported elsewhere [34–37]. The computed optical properties are shown in Fig. 6. The real dielectric function describes the polarisation characteristics of a material, whereas the imaginary dielectric function defines the ability of the material to absorb light [38]. Fig. 6(a) shows the appearance of the highest ε1 (ω) peak for K_2SbAu (8.8) at 1.76 eV. Thereafter, the $\varepsilon_1(\omega)$ spectra decrease with an increase in energy and attain negative values in the 5.5–6.6 eV energy range when K_2SbAu is reflective. The static dielectric function ε_1 (0) describes the magnitude of charge recombination in the materials. Higher dielectric functions imply reduced recombination of charges within a material and vice versa [38]. The ε_1 (0) value obtained for K_2SbAu was 6.46, suggesting weaker charge recombination and, hence, enhanced optoelectronic performance. The $\varepsilon_2(\omega)$ peaks describe the interband transitions from the valence band to the conduction band within a material. The $\varepsilon_2(\omega)$ spectral threshold is consistent with the computed GGA band gap of 1 eV in the visible region. This narrow band gap is desirable for faster charge transfer, making the K_2SbAu compound suitable for solar cell applications. The $\varepsilon_2(\omega)$ spectra increase with the increase in energy and attain their highest value of 22.3 at 2.42 eV, and thereafter decrease exponentially. As anticipated, the n(ω) spectra (Fig. 6(b)) resembled $\varepsilon_1(\omega)$ in Fig. 6(a). The initial value of the refractive index of K_2SbAu is 2.54. Beyond this value, the n(ω) spectra increase with increasing energy, attaining a maximum of 3.78 at 2.42 eV. Above

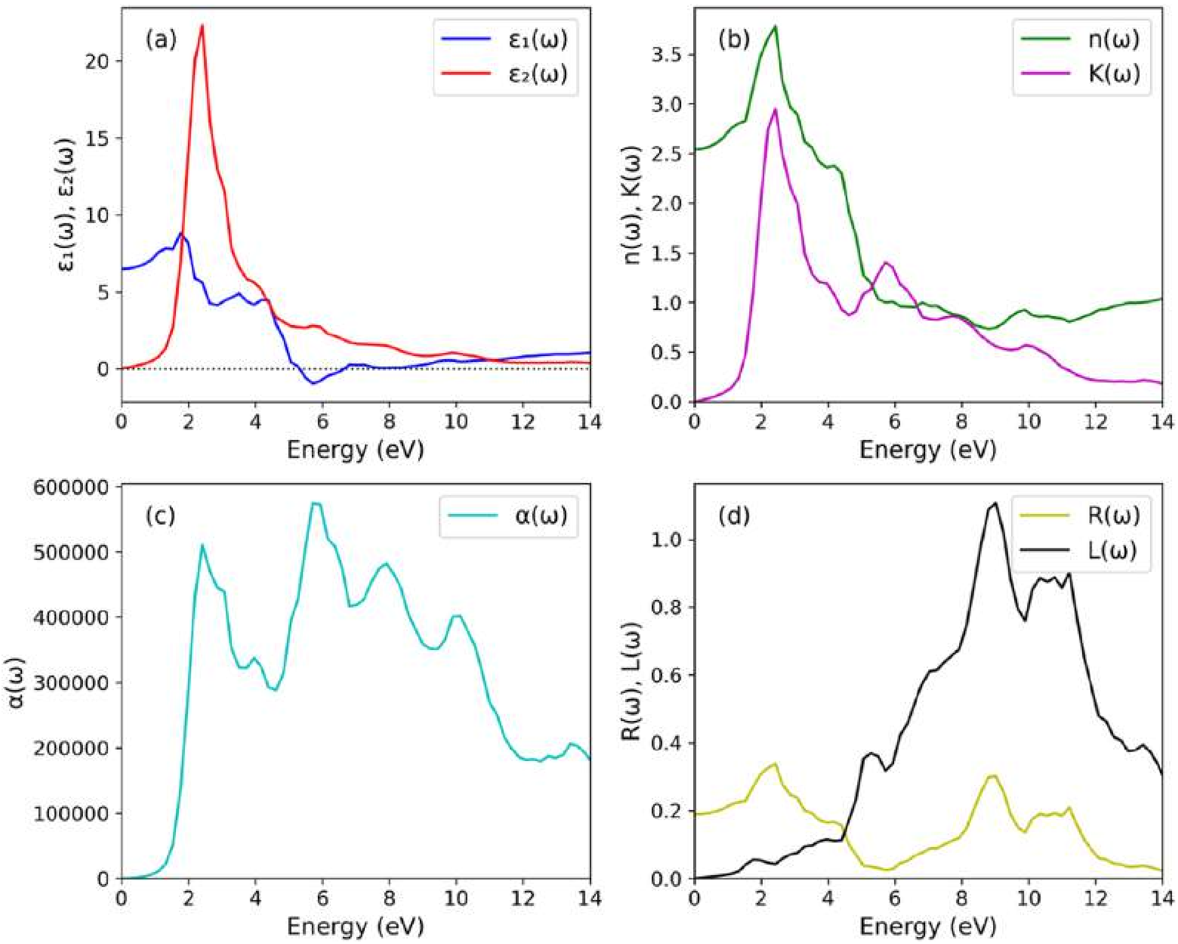

Fig. 6. Optical properties of K_2SbAu ternary compound computed using GGA approximation. (a) $\varepsilon_1(\omega)$ and $\varepsilon_2(\omega)$, (b) n(ω) and K(ω), (c) α(ω), and (d) R(ω) and L(ω).

this photon energy, the n(ω) spectra decreased. Similarly, the K(ω) spectra increase from zero energy, reach the highest value of 2.95 at 2.42 eV, and decline thereafter with an increase in photon energy. The α(ω) provides valuable insights into optical energy absorption per unit length [39]. Optical absorption occurs when the frequency of an incoming photon resonates with the transition frequency of an atom. Optical absorption involves an electron transition from the valence band to the conduction band. Fig. 6(c) shows that the α(ω) threshold reflects a band gap of approximately 1 eV in the near-infrared region, implying the high transparency of K_2SbAu to near-infrared light. The α(ω) spectra experienced growth from the threshold point and remained high in the 2–10 eV energy region. This high absorption in the ultraviolet–visible region is desirable for optimum light absorption, making K_2SbAu a suitable absorber for light energy devices. Reflectivity describes the ability of a material to reflect energy from its surface [40]. As shown in Fig. 6(d), the static reflectivity, R (0), was 0.19. The R(ω) spectra increase with increasing energy, attaining a maximum of 0.52 at 2.41 eV. This shows that photon reflection grows with an increase in energy. Beyond 2.41 eV, the reflectivity decreases. The L(ω) describes an inelastic scattering process in materials [41]. Fig. 6(d) shows that inelastic scattering is insignificant in the low-energy regions. Analyses of Fig. 6(c) and (d) suggest that the threshold values of the α(ω) and the L(ω) are in good agreement, implying that the scattering process becomes more prominent when the K_2SbAu ternary compound absorbs incident light. The L(ω) spectra increase exponentially with energy, attaining a maximum of 1.1 at 9 eV, and then decrease. Overall, across the ultraviolet–visible region (0–14 eV), the K_2SbAu ternary compound shows good optical properties that are desirable for photovoltaic applications.

3.6. *Thermoelectric properties*

The Seebeck coefficient (S), electrical conductivity (σ/τ), and electronic thermal conductivity (k_e/τ) were calculated utilising the BoltzTraP code [42] within the 100–800 K temperature range. The Seebeck coefficient represents the majority carrier in a material [43]. As shown in Fig. 7(a), the Seebeck coefficient values obtained for the K_2SbAu ternary compound are positive, implying that most charge carriers are holes; thus, they are p-type semiconductors. The Seebeck coefficient increased with increasing temperature. At approximately 500 K, the Seebeck coefficient for K_2SbAu attains its highest value of 238 μV/K; beyond 500 K, it decreases. This behaviour depends on the material's variables, and in some materials, it might be favourable for thermoelectric field applications. Fig. 7(b) shows the electronic conductivity of the K_2SbAu ternary compound. The plot shows that the electronic conductivity also increased as the temperature increased. This increase in electronic conductivity suggests semiconducting behaviour. At 800 K, the highest recorded value of electronic conductivity was 4.66×10^{18} $(\Omega ms)^{-1}$. This trend can be attributed to an increase in temperature, which increases the charge carrier density. Fig. 7(c) shows the electrical thermal conductivity of the K_2SbAu ternary compound. The electrical thermal conductivity increased with temperature over the 100–800 K temperature range. At 100 K, it exponentially increases from 1.73×10^{12} to the highest value of 2.8×10^{14} W/Kms at 800 K. The lattice thermal conductivity κl was computed using the phono3py module [44] and Quantum Espresso. The lattice thermal conductivity in Fig. 7(d) shows an inverse relationship with temperature. As temperature increases from 100 K to 800 K, kl decreases monotonically from 1.27×10^6 W/Kms to 1.23×10^5 W/Kms. This decrease in kl is attributed to increased phonon

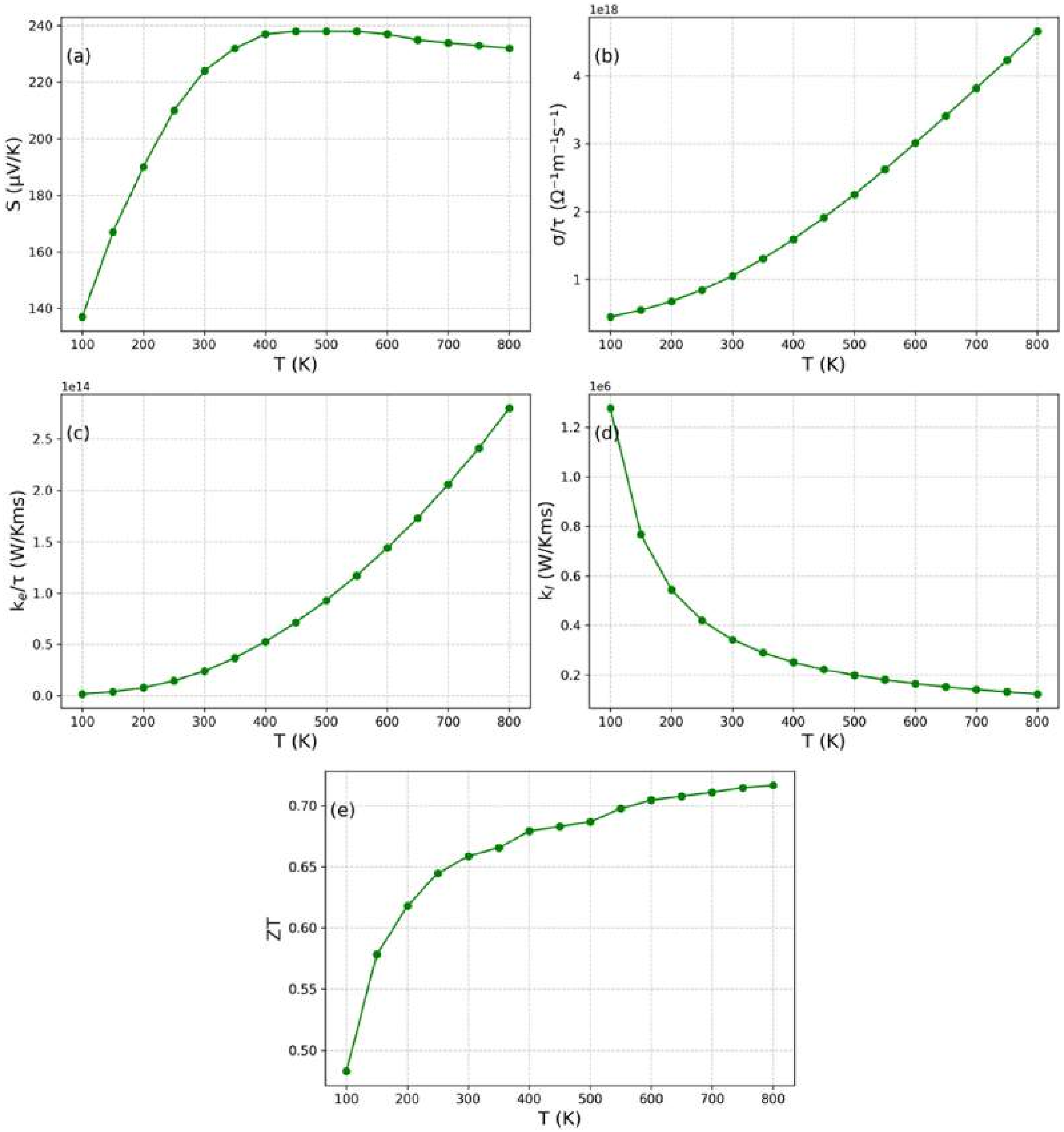

Fig. 7. The thermoelectric properties of the K_2SbAu ternary compound. (a) Seebeck coefficient (S), (b) Electrical conductivity (σ/τ), (c) Electronic thermal conductivity (k_e/τ), (d) Lattice thermal conductivity (kl), and (e) Figure of merit (ZT).

scattering [45]. The low kl contributes to enhanced thermoelectric efficiency of materials to convert heat into electricity [46].) Fig. 7(e) depicts the temperature-dependent dimensionless figure of merit of the K_2SbAu ternary compound. The figure of merit describes the power-generation efficiency of thermoelectric devices, defined as $ZT = S^2\sigma T/K$ [47]. K is the sum of the electronic and lattice thermal conductivities. ZT steadily increases for the 100–800 K temperature range, reaching the highest value of 0.71. This indicates that the K_2SbAu ternary compound can be used in the thermoelectric field.

Fig. 8 displays the chemical potential-dependent thermoelectric properties of K_2SbAu at temperatures ranging from 100 to 800 K using GGA-PBE. The Seebeck coefficient shown in Fig. 8(a) varies between 0.2 and 2.6 mV/K near the Fermi level (5.0 eV). All Seebeck coefficient values for K_2SbAu are positive at the Fermi level, indicating a p-type semiconductor. The perpendicular component of S is greater in magnitude, which is advantageous for thermoelectric properties. The electrical and electronic thermal conductivities approach zero around the Fermi level and increase as the temperature rises.

4. Conclusion

Using first-principles methods, we thoroughly investigated the structural, electronic, elastic, optical, and thermoelectric properties of a K_2SbAu ternary compound. The negative enthalpy of formation indicates that this compound is thermodynamically stable and can be experimentally synthesised. Band structure and projected density of states calculations indicate that the compound is a semiconductor with an indirect band gap ranging from 0.78 to 1.84 eV, desirable for optoelectronic applications. The projected density of states further shows that the Au3*d* and Sb2*p* states primarily form the valence band, whereas the Au2*p* states dominate the formation of conduction bands in the K_2SbAu ternary compound. The K_2SbAu ternary compound fulfilled Born's elastic stability criterion, establishing its mechanical stability. Considering its Pugh and Poisson ratios, the studied compound displays

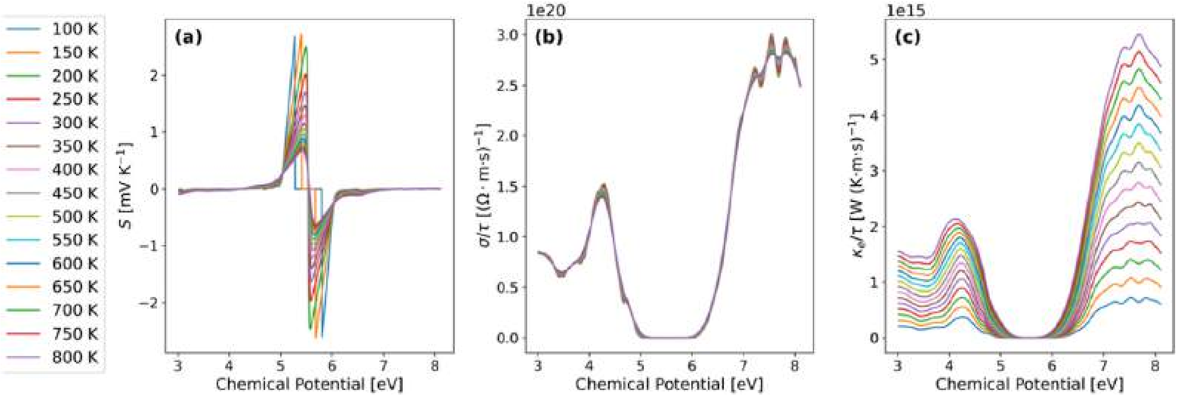

Fig. 8. The thermoelectric properties of the K_2SbAu ternary compound. (a) Seebeck coefficient (S), (b) Electrical conductivity (σ/τ), (c) Electronic thermal conductivity (k_e/τ) as a function of chemical potential.

ductile and ionic characteristics. With high absorption coefficient values in the ultraviolet–visible spectrum, the K_2SbAu ternary compound is suitable for optoelectronic applications such as solar cells. The K_2SbAu ternary compound appears to be well-suited for thermoelectric applications because of the high values observed for the Seebeck coefficients, electrical conductivity, and figure of merit. This study advances our understanding of the K_2SbAu ternary compound and contributes to ongoing efforts to discover and develop zintl phases with excellent qualities for optoelectronic and thermoelectric applications.

CRediT authorship contribution statement

Ibrahim Musanyi: Writing – review & editing, Writing – original draft, Methodology, Investigation, Formal analysis, Data curation, Conceptualization. **Mwende Mbilo:** Writing – review & editing, Writing – original draft, Validation, Investigation, Formal analysis, Data curation, Conceptualization. **Robinson Musembi:** Writing – review & editing, Writing – original draft, Visualization, Validation, Supervision, Software, Resources, Project administration, Methodology, Investigation, Funding acquisition, Formal analysis, Data curation, Conceptualization. **John Kachira:** Writing – review & editing, Writing – original draft, Methodology, Investigation, Formal analysis, Data curation. **Francis Nyongesa:** Writing – review & editing, Writing – original draft, Validation, Supervision, Formal analysis, Data curation. **Martin Nyamunga:** Writing – review & editing, Writing – original draft, Methodology, Investigation, Data curation. **Samuel Wafula:** Writing – review & editing, Writing – original draft, Methodology, Investigation, Data curation.

Data availability

The data will be available upon request.

Declaration of competing interest

The authors declare that they have no known competing financial interests or personal relationships that could have appeared to influence the work reported in this paper.

Acknowledgements

The authors acknowledge the University of Nairobi for its resources in doing this work and the Centre for High-Performance Computing (CHPC-RSA) for its computing resources through account number MATS1321.

Data availability

Data will be made available on request.

References

[1] M. Victoria, et al., Solar photovoltaics is ready to power a sustainable future, Joule 5 (5) (2021) 1041–1056, https://doi.org/10.1016/j.joule.2021.03.005.
[2] D. Behera, R. Sharma, H. Ullah, H.S. Waheed, S.K. Mukherjee, Electronic, optical, and thermoelectric investigations of Zintl phase AAg2Se2 (A=Sr, Ba) compounds: a first-principle approach, J. Solid State Chem. 312 (2022) 123259, https://doi.org/10.1016/j.jssc.2022.123259.
[3] A.I. Aljameel, et al., Investigation of optoelectronic and thermoelectric properties of novel BaCd2X2 (X = P, As, Sb) Zintl-phase for energy harvesting applications, J. Phys. Chem. Solid. 189 (2024) 111953, https://doi.org/10.1016/j.jpcs.2024.111953.
[4] A.N. Rima, M. Atikur Rahman, R. Ferdous, M.N.M. Nobin, M.F. Rahman, DFT simulation to study the physical properties of ternary intermetallic materials ACuSb (A=Ca, Sr, Ba) for solar cell and TBC materials, Comput. Condens. Matter 39 (2024) e00900, https://doi.org/10.1016/j.cocom.2024.e00900.
[5] J. Zhang, et al., Designing high-performance layered thermoelectric materials through orbital engineering, Nat. Commun. 7 (2016) 1–7, https://doi.org/10.1038/ncomms10892.
[6] U. Hameed, et al., First-principles calculations to investigate magnetic, electronic, and thermoelectric response of europium-based half metallic ternary Zintl compounds EuMg2X2 (X=Sb and Bi), J. Phys. Chem. Solid. 199 (2025) 112519, https://doi.org/10.1016/j.jpcs.2024.112519.
[7] A. Youcef, et al., Topologically nontrivial phase in Na2CuX (X= As, Sb, Sn and Bi) full Heusler compounds: insights from DFT-based computer simulation, Rev. Mexic. Fisica 69 (2) (2023) 1–8, https://doi.org/10.31349/RevMexFis.69.020501.
[8] G. Savelsberg, H. Schäfer, Darstellung und Kristallstruktur von Na2CuP, K2AgAs, K2AgSb und K2AgBi, Zeitschrift fur Naturforsch. - Sect. B J. Chem. Sci. 32 (7) (1977) 745–748, https://doi.org/10.1515/znb-1977-0704.
[9] C. Structure, K. C. A, K. C. S, Nur Vorhanden Für, 1976, pp. 10–12.
[10] M. Asbrand, B. Eisenmann, M. Somer, No title, Z. Kristallogr. New Cryst. Struct. 212 (1) (1997) 78, https://doi.org/10.1524/ncrs.1997.212.1.78.
[11] S. Maabed, M. Halit, A. Bouhemadou, A. Benmakhlouf, M. Bouchenafa, Equilibrium ground-state properties of the ternary alkali metal coinage metal phosphides K2CuP and K2AgP: new insights from first principles calculations, J. Alloys Compd. 804 (2019) 128–138, https://doi.org/10.1016/j.jallcom.2019.07.013.
[12] R. Musembi, M. Mbilo, M. Nyamuga, J. Kachila, Analysis of Na2CuP ternary semiconductor compound for optoelectronic application by first-principles methods using GGA and mGGA functionals, Comput. Condens. Matter 40 (April) (2024) e00927, https://doi.org/10.1016/j.cocom.2024.e00927.
[13] C. Zeng, et al., Total structure and electronic properties of the gold nanocrystal Au 36(SR) 24, Angew. Chem. Int. Ed. 51 (52) (2012) 13114–13118, https://doi.org/10.1002/anie.201207098.
[14] S. Kim, G.J. Miller, J.D. Corbett, Zigzag chains of alternating atoms in A2AuBi (A = Na, K) and K2AuSb. Synthesis, structure, and bonding, Z. Anorg. Allg. Chem. 636 (2010) 67–73 [Online]. Available: https://api.semanticscholar.org/CorpusID:96664402.
[15] P. Honenberg, W. Kohn, Inhomogeneous electron gas, Phys. Rev. 136 (3B) (1964) 1–8, https://doi.org/10.1007/BF01198136.
[16] P. Giannozzi, et al., Quantum espresso: a modular and open-source software project for quantum simulations of materials, J. Phys. Condens. Matter 21 (39) (2009) 395502, https://doi.org/10.1088/0953-8984/21/39/395502.
[17] J.P. Perdew, K. Burke, M. Ernzerhof, Generalized gradient approximation made simple, Phys. Rev. Lett. 77 (18) (1996) 3865–3868, https://doi.org/10.1103/PhysRevLett.77.3865.

[18] P. Ziesche, S. Kurth, J.P. Perdew, Density functionals from LDA to GGA, Comput. Mater. Sci. 11 (2) (1998) 122–127, https://doi.org/10.1016/S0927-0256(97)00206-1.

[19] A.P. Bartók, J.R. Yates, Regularized SCAN functional, J. Chem. Phys. 150 (16) (2019) 1–6, https://doi.org/10.1063/1.5094646.

[20] D. Koller, F. Tran, P. Blaha, Improving the modified Becke-Johnson exchange potential, Phys. Rev. B Condens. Matter 85 (15) (2012) 1–8, https://doi.org/10.1103/PhysRevB.85.155109.

[21] T. Maeda, S. Nakamura, T. Wada, First principles calculations of defect formation in in-free photovoltaic semiconductors Cu2ZnSnS4 and Cu2ZnSnSe 4, Jpn. J. Appl. Phys. 50 (2011) 2–7, https://doi.org/10.1143/JJAP.50.04DP07.

[22] H. Bennacer, A. Boukortt, S. Meskine, M. Hadjab, M.I. Ziane, A. Zaoui, First principles investigation of optoelectronic properties of ZnXP2 (X = Si, Ge) lattice matched with silicon for tandem solar cells applications using the mBJ exchange potential, Optik 159 (2018) 229–244, https://doi.org/10.1016/j.ijleo.2018.01.079.

[23] M. Mbilo, R. Musembi, First principles calculation to investigate the structural, electronic, elastic, mechanical, and optical properties of K2NiP2ternary compound, AIP Adv. 12 (2022) 105018, https://doi.org/10.1063/5.0118809.

[24] T. Atsue, I.B. Ogunniranye, O.E. Oyewande, Investigation of material properties of halide mixed lead - free double perovskite for optoelectronic applications using first-principles study, Mater. Sci. Semicond. Process. 133 (May) (2021) 105963, https://doi.org/10.1016/j.mssp.2021.105963.

[25] S. Bağci, S. Duman, H.M. Tütüncü, G.P. Srivastava, Electronic and phonon properties of BX (110) (X=P, As, and Sb) and BeY (110) (Y=S, Se, and Te) surfaces, Phys. Rev. B Condens. Matter 79 (12) (2009) 1–13, https://doi.org/10.1103/PhysRevB.79.125326.

[26] K.S. Jin, G.J. Miller, J.D. Corbett, Zigzag chains of alternating atoms in A2 Au Bi (A = Na, K) and K2 Au Sb. Synthesis, structure, and bonding, Zeitschrift fuer Anorg. und Allg. Chemie 636 (2010) 67–73.

[27] F. Mouhat, F.X. Coudert, Necessary and sufficient elastic stability conditions in various crystal systems, Phys. Rev. B Condens. Matter 90 (22) (2014) 1–4, https://doi.org/10.1103/PhysRevB.90.224104.

[28] D. Hong, W. Zeng, F.-S. Liu, B. Tang, Q.-J. Liu, The structural, mechanical and electronic properties of NbXSi (X=Fe, Co, Ni, Ru, Rh, Pd, Os, Ir and Pt) compounds from first-principles calculations, Mater. Chem. Phys. 259 (2021) 124029, https://doi.org/10.1016/j.matchemphys.2020.124029.

[29] R.K. Pingak, et al., Structural, electronic, elastic, and optical properties of cubic BaLiX3 (X = F, Cl, Br, or I) perovskites: an ab-initio DFT study, Indones. J. Chem. 23 (3) (2023) 843–862, https://doi.org/10.22146/ijc.83261.

[30] V. Kumar, B.P. Singh, Structural and elastic properties of AIBIIIC 2VI semiconductors, Indian J. Phys. 92 (1) (2018) 29–35, https://doi.org/10.1007/s12648-017-1082-3.

[31] Z. Abbas, et al., DFT insights for structural, opto-electronic, thermodynamic and transport characteristics of Tl2TeX6 (X = At, Br, Cl, I) double perovskites for low-cost solar cell applications, Inorg. Chem. Commun. 163 (December 2023) (2024) 112293, https://doi.org/10.1016/j.inoche.2024.112293.

[32] R. Bhattacharjee, S. Chattopadhyaya, Effects of barium (Ba) doping on structural, electronic and optical properties of binary strontium chalcogenide semiconductor compounds - a theoretical investigation using DFT based FP-LAPW approach, Mater. Chem. Phys. 199 (2017) 295–312, https://doi.org/10.1016/j.matchemphys.2017.06.057.

[33] A. Srivastava, P. Sarkar, S.K. Tripathy, T.R. Lenka, P.S. Menon, Structural, electronic and optical properties of Ag2MgSn(S/Se)4 quaternary chalcogenides as solar cell absorber layer: an Ab-initio study, Sol. Energy 209 (August) (2020) 206–213, https://doi.org/10.1016/j.solener.2020.08.094.

[34] Y.O. Ciftci, K. Colakoglu, N.S. Korozlu, First principles studies of elastic, electronic and optical properties of chalcopyrite semiconductor ZnSnP 2, J. Alloys Compd. 529 (2012) 1–7, https://doi.org/10.1016/j.jallcom.2012.03.046.

[35] G. Nazir, S. Tariq, A. Afaq, Q. Mahmood, Under pressure DFT investigations on optical and electronic properties of PbZrO3, Acta Phys. Pol., A 133 (1) (2018) 105–113, https://doi.org/10.12693/APhysPolA.133.105.

[36] F. Okbi, S. Lakel, S. Benramache, K. Almi, First principles study on electronic structure and optical properties of ternary semiconductor InxAl1 –xP alloys, Semiconductors 54 (1) (2020) 58–66, https://doi.org/10.1134/S1063782620010182.

[37] M.S. Yaseen, J. Sun, H. Fang, G. Murtaza, D.S. Sholl, First-principles study of electronic and optical properties of ternary compounds AuBX2 (X = S, Se, Te) and AuMTe2 (M = Al, In, Ga), Solid State Sci. 111 (2021) 106508, https://doi.org/10.1016/j.solidstatesciences.2020.106508.

[38] D. Abdullah, D.C. Gupta, Analyzing the structural, optoelectronic, and thermoelectric properties of InGeX3 (X = Br) perovskites via DFT computations, Sci. Rep. 14 (1) (2024) 23575, https://doi.org/10.1038/s41598-024-72745-w.

[39] H. M, E. R.D, Investigations on the thermoelectric and thermodynamic properties of quaternary coinage metal HgSBr, Heliyon 9 (9) (2023) e19438, https://doi.org/10.1016/j.heliyon.2023.e19438.

[40] N. Rahman, et al., Appealing perspectives of the structural, electronic, elastic and optical properties of LiRCl3 (R = Be and Mg) halide perovskites: a DFT study, RSC Adv. 13 (27) (2023) 18934–18945, https://doi.org/10.1039/d3ra02640j.

[41] M.Z. Rana, M.R. Munshi, M. Al Masud, M.S. Zahan, Structural, electronic, optical and thermodynamic properties of AlAuO2 and AlAu094Fe006O2 compounds scrutinized by density functional theory (DFT), Heliyon 9 (11) (2023) e21405, https://doi.org/10.1016/j.heliyon.2023.e21405.

[42] G.K.H. Madsen, D.J. Singh, BoltzTraP. A code for calculating band-structure dependent quantities, Comput. Phys. Commun. 175 (1) (2006) 67–71, https://doi.org/10.1016/j.cpc.2006.03.007.

[43] M. Manzoor, D. Behera, R. Sharma, A.J.A. Moayad, A.A. Al-Kahtani, Y. Anil Kumar, Comprehensive first principles to investigate optoelectronic and transport phenomenon of lead-free double perovskites Ba2AsBO6 (B[dbnd]Nb, Ta) compounds, Heliyon 10 (9) (2024) e30109, https://doi.org/10.1016/j.heliyon.2024.e30109.

[44] A. Togo, L. Chaput, T. Tadano, I. Tanaka, Implementation strategies in phonopy and phono3py, J. Phys. Condens. Matter 35 (35) (2023) 353001, https://doi.org/10.1088/1361-648X/acd831.

[45] K. Shen, et al., Point defects enhance cross-plane thermal conductivity in graphite, Adv. Mater. (2025) 2418569, https://doi.org/10.1002/adma.202418569, 1–9.

[46] X. Huang, K. Luo, Y. Shen, Y. Yue, Q. An, Grain boundaries induce significant decrease in lattice thermal conductivity of CdTe, Energy AI 11 (July 2022) 4–11, https://doi.org/10.1016/j.egyai.2022.100210, 2023.

[47] S. Irfan, Z. Yan, S.B. Khan, Advancements in thermoelectric materials: a comprehensive review, Mater. Sci. Energy Technol. 7 (June) (2024) 349–373, https://doi.org/10.1016/j.mset.2024.06.002.